Acta Oceanol. Sin., 2010, Vol.29, No.1, p.88-99
DOI: 10.1007/s13131-010-0011-5
http://www.hyxb.org.cn
E-mail: hyxbe@263.net

Numerical study on the characteristics of flow field and wave propagation near submerged breakwater on slope

CHEN Jie[1,2*], JIANG Changbo[1,2], HU Shixiong[3], HUANG Wenwei[4]

[1] School of Hydraulic Engineering, Changsha University of Science & Technology, Changsha 410114, China

[2] Hunan Province Key Laboratory of Water, Sediment Sciences & Flood Hazard Prevention, Changsha 410114, China

[3] Department of Geography, East Stroudsburg University of Pennsylvania, East Stroudsburg, PA 18301, USA

[4] School of Foreign Languages, Changsha University of Science & Technology, Changsha 410114, China

Received 19 December 2008; accepted 14 July 2009

Abstract
In this study, characteristics of flow field and wave propagation near submerged breakwater on a sloping bed are investigated with numerical model. The governing equations of the vertical two-dimensional model are Reynolds Averaged Navier Stokes equations. The Reynolds stress terms are closed by a nonlinear $k-\varepsilon$ turbulence transportation model. The free surface is traced through the PILC-VOF method. The proposed numerical model is verified with experimental results. The numerical result shows that the wave profile may become more asymmetrical when wave propagates over breakwater. When wave crest propagates over breakwater, the anticlockwise vortex may generate. On the contrary, when wave hollow propagates over breakwater, the clockwise vortex may generate. Meanwhile, the influenced zone of vortex created by wave crest is larger than that created by wave hollow. All the maximum values of the turbulent kinetic energy, turbulent dissipation and eddy viscosity occur on the top of breakwater. Both the turbulent dissipation and eddy viscosity increase as the turbulent kinetic energy increases. Wave energy may rapidly decrease near the breakwater because turbulent dissipation increases and energy in lower harmonics is transferred into higher harmonics.

Key words: submerged breakwater, characteristics of flow field, PLIC-VOF method, sloping bed

1 Introduction

With the development of economy in China, the dynamic equilibrium of the coastal region has been disturbed and serious coastal erosion and accretion occurred. As a severe problem worldwide, coastal erosion endangered the coastal properties, and caused degradation of valuable land and natural resources, and produced the disruption to fishing, shipping and tourism. The development of coastal facilities requires proper management of the sea front, which can warrant the construction of coastal protective structures. The submerged breakwaters have become increasingly popular due to their multiple functions, which are to protect shoreline or harbor and to prevent beach erosion in the coastal zones. The main function of these breakwaters is to protect the seaward area from the severe wave actions by attenuating the wave pass over the structure. Submerged breakwaters could absorb some of incoming wave energy by causing the wave to break prematurely, thus diminishing the transmitted wave energy.

Due to the engineering importance of the breakwaters mentioned above, laboratory researches have tended to focus on the interactions between breaking solitary wave (Grilli et al., 1994), non-breaking regular wave (Losada et al., 1996), directional random wave (Losada et al., 1996), multi-directional random wave (Hur et al., 2003; Hur, 2004) and submerged breakwaters. Stamos et al. (2001, 2003) carried out

Foundation item: The National Natural Science Foundation of China under contract Nos 50979008 and 50909009; Program for Hunan Province Key Laboratory of Water, Sediment Sciences & Flood Hazard Prevention and Open Research Fund Program of State Key Laboratory of Hydrology-Water Resources and Hydraulic Engineering, Hohai University No.2008490911.
*Corresponding author, E-mail: chenjie166@yahoo.com.cn

experimental study to compare the reflection and transmission characteristics of submerged hemicylindrical, rectangular rigid and water-filled flexible breakwatermodels. The strong reflection of regular water wave over a trai n of submerged breakwaters also was inves-tigated by the series of laboratory experiments (Cho et al., 2004). Recently, Cox and Tajziehchi (2005) performed experiments to explore the overtopping flow across submerged breakwater with different crest widths under different submergences. Analysis of data showed that flux was influenced most by breakwater crest width rather than other variables. Jeng et al. (2005) conducted laboratory experiments and recorded the water surface elevation and the pore pressures inside the seabed foundations to investigate interaction between water wave, a submerged breakwater, a vertical wall and a sandy seabed.

As experimentally studies have been widely carried out, computationally numerical models have also been wisely used to predict interactions between wave and submerged breakwaters (e.g., Mizutani et al., 1998; Chen et al., 2004; Johnson et al., 2005; Chen et al., 2006; Johnson, 2006; Kobayashi et al., 2007). Mizutani et al. (1998) developed numerical and physical models to study the nonlinear dynamic interaction between water wave and permeable submerged breakwater over a finite thickness sand seabed. Rambabu and Mani (2005) used a numerical model to study the transmission characteristics of a submerged breakwater and to determine the effects of the depth of submergence, crest width, initial wave conditions and material properties on the transmission characteristics of the submerged breakwater. The results highlighted the optimum crest width of the breakwater and optimum clear spacing between two breakwaters. The interaction between nonlinear wave and submerged breakwaters was numerical simulated (Liu et al., 2005; Zhou et al., 2005). The fluid solver was based on a method for Navier-Stokes equation. The free surface of wave was traced through the PLIC-VOF (Liu et al., 2005). Recently, Kobayashi et al. (2007) used a numerical model based on time-averaged continuity, momentum, and energy equations to predict the mean and standard deviation of the free surface elevation and horizontal fluid velocities above and inside a porous submerged breakwater. In addition, the experimental and numerical investigations have been widely performed to analyze wave interaction with breakwaters (Losada et al., 2004; Reddy et al., 2007).

However, most studies on wave propagation over submerged breakwater were based on the plane bed (e.g., Grilli et al., 1994; Cox and Tajziehchi, 2005; Liu et al., 2005; Zhou et al., 2005). In fact, submerged breakwaters were mostly located near shore. Wave propagation would be influenced by shoaling as the depth of water decreases. Studies of interactions between wave and submerged breakwaters on the sloping bed could be fully applied to investigate the essential characteristics in practice. Although some studies of wave propagation over submerged breakwater installed on a sloping bed have been performed (e.g., Losada et al., 1996; Hur, 2003, 2004; Kobayashi et al., 2007; Jiang et al., 2008; Chen et al., 2008), it is recently short of studies in this domain especially lacking of investigations on changes of characteristics of flow field at front and back of submerged breakwater on the slope.

In order to investigate characteristics of flow field and wave propagation near submerged breakwater on a sloping bed, a numerical model is developed in this study. In the numerical model, the two-dimensional numerical wave flume is solved by the PLIC-VOF technique. Based on the developed model which was verified by the experimental data, the changes of wave propagation, wave surface, velocity field, turbulent kinetic energy, turbulent dissipation and eddy viscosity at front and back of the submerged breakwater on the slope are investigated.

2 The numerical model

2.1 *Governing equations*

PLIC-VOF model is more flexible and efficient than other methods for treating arbitrary free boundaries in a wide range of applications. It is used for the analysis of wave field in this study. Based on the PLIC-VOF method, a numerical wave flume is developed and applied to the simulation of the wave motion. The fluid is considered to be viscous and incompressible. The numerical model solves the Reynolds Averaged Navier Stokes equations, with a nonlinear $k-\varepsilon$ turbulence model. The governing equations used in the calculation are, the continuity equation, the momentum equations as follows:

Continuity equation:

$$\frac{\partial \overline{u_i}}{\partial \overline{x_i}} = 0. \tag{1}$$

Momentum equation:

$$\frac{\partial \overline{u_i}}{\partial t} + \overline{u_j}\frac{\partial \overline{u_i}}{\partial x_j} = -\frac{1}{\rho}\frac{\partial \overline{p}}{\partial x_i} + g_i + \frac{1}{\rho}\frac{\partial \overline{\tau_{ij}}}{\partial x_j}, \tag{2}$$

where i, j=1,2 for each of the fluid dimensions. U_i represents the i-th component of velocity vector, ρ is the density, p the pressure, g_i the i-th component of the gravity acceleration and g_i the viscous stresses. Likewise $\tau_{ij} = 2\mu S_{ij} + \rho\overline{u_i'u_j'}, S_{ij} = \frac{1}{2}(\frac{\partial\overline{u_i}}{\partial x_j} + \frac{\partial\overline{u_j}}{\partial x_i}), \mu = v\rho$ is the dynamic viscosity and v is the kinematic viscosity.

$k-\varepsilon$ turbulence model:

$$\frac{\partial k}{\partial t} + \overline{u_j}\frac{\partial k}{\partial x_j} = \frac{\partial}{\partial x_j}[(\frac{v_t}{\sigma_k} + v)\frac{\partial k}{\partial x_j}] - \overline{u_i'u_j'}\frac{\partial\overline{u_i}}{\partial x_j} - \varepsilon, \tag{3}$$

$$\frac{\partial \varepsilon}{\partial t} + \overline{u_j}\frac{\partial \varepsilon}{\partial x_j} = \frac{\partial}{\partial x_j}[(\frac{v_t}{\sigma_\varepsilon} + v)\frac{\partial \varepsilon}{\partial x_j}] + 2C_{1\varepsilon}\frac{\varepsilon}{k}v_t S_{ij}\frac{\partial\overline{u_i}}{\partial x_j} - C_{2\varepsilon}\frac{\varepsilon^2}{k}. \tag{4}$$

Nonlinear closure model:

$$\overline{u_i'u_j'} = \frac{2}{3}k\delta_{ij} - C_d\frac{k^2}{\varepsilon}(\frac{\partial\overline{u_i}}{\partial x_j} + \frac{\partial\overline{u_j}}{\partial x_i}) - \frac{k^3}{\varepsilon^2}[C_1(\frac{\partial\overline{u_i}}{\partial x_l}\frac{\partial\overline{u_l}}{\partial x_j} + \frac{\partial\overline{u_j}}{\partial x_l}\frac{\partial\overline{u_l}}{\partial x_i} - \frac{2}{3}\frac{\partial\overline{u_l}}{\partial x_k}\frac{\partial\overline{u_k}}{\partial x_l}\delta_{ij}) + C_2(\frac{\partial\overline{u_i}}{\partial x_k}\frac{\partial\overline{u_j}}{\partial x_k} - \frac{1}{3}\frac{\partial\overline{u_l}}{\partial x_k}\frac{\partial\overline{u_l}}{\partial x_k}\delta_{ij}) + C_3(\frac{\partial\overline{u_k}}{\partial x_i}\frac{\partial\overline{u_k}}{\partial x_j} - \frac{1}{3}\frac{\partial\overline{u_l}}{\partial x_k}\frac{\partial\overline{u_l}}{\partial x_k}\delta_{ij})], \tag{5}$$

where $k = \overline{u_i'u_i'}/2$ is turbulent kinetic energy, $\varepsilon = v\frac{\partial u_i'\partial u_i'}{\partial x_k\partial x_k}$ is turbulent dissipation rate, $v_t = C_d\frac{\kappa^2}{\varepsilon}$ is eddy viscosity, σ_k=1.0, σ_ε=1.3, $C_{1\varepsilon}$=1.44, $C_{2\varepsilon}$=1.92, $C_d = \frac{2}{3}(\frac{1}{7.4+S_{\max}})$, and $S_{\max} = \frac{\kappa}{\varepsilon}\max(|\frac{\partial\overline{u_i}}{\partial x_i}|)$.

In PLIC-VOF method, a fraction function $F(x, y, t)$ is introduced to describe the fluid volume in a cell. A unit value of F corresponds to a cell full of fluid, whereas a zero value indicates the cell contains no fluid. Cells with an F value between zero and one are either intersected by a free surface or be composed of voids (bubbles) smaller than cell mesh dimensions. The time dependence of F is governed by:

$$\frac{\partial F}{\partial t} + \frac{\partial}{\partial x}(\theta uF) + \frac{\partial}{\partial z}(\theta vF) = 0, \tag{6}$$

where F is the fluid volume function.

The computational mesh is rectangular, and the cells spacing can be varied. The nodes for the horizontal and the vertical velocities (U, V) are at the midpoint of the vertical and the horizontal sides of the cell, whereas those for the other variables (p, F and ρ) are at the center of the cell. Eq. (1) is discretized by a space-central difference scheme. Eq. (2) is discretized by a central difference scheme in time term and donor upwind scheme in space term. And Eq. (6) is specially handled by PLIC-VOF method because $F(x, y, t)$ is a step function and cannot be discretized in a usual way.

2.2 *PLIC-VOF Model*

The PLIC-VOF algorithm simulates the free surface in two steps, an interface reconstruction step and a flow propagation step. Typical interface reconstruction and flow propagation are shown in Fig. 1. It is assumed that the free surface is made up of many lines in cells with F between 0 and 1, and that these lines intersect the boundaries of cells at many points. After capturing all these points, PLIC-VOF can predict the convection of the fluid according to the direction of free surface and its velocity. After the velocity field is computed by PLIC-VOF, a reconstruction of free surface and flow propagation could be completed with a splitting algorithm in x and y directions alternately under the Courant-Friedrichs-Lewy condition.

In SLIC-VOF, a horizontal or vertical line in a cell with an F value between 0 and 1 represents the free surface. Whether the line is horizontal or vertical in a surface cell depends on the local slope of the fluid interface. The advantages of PLIC-VOF can be shown by a simple case shown in Fig.2. The dashed line in Fig. 2 is the true interface, the number in each cell is volume fraction at each time step, and the shaded part in each cell is an approximation of the free surface. It is generally recognized that flux advection between surface cells in PLIC-VOF is more precise than that in SLIC-VOF, and the pressure and velocity computed by PLIC-VOF are mere accurate than that computed by SLIC-VOF.

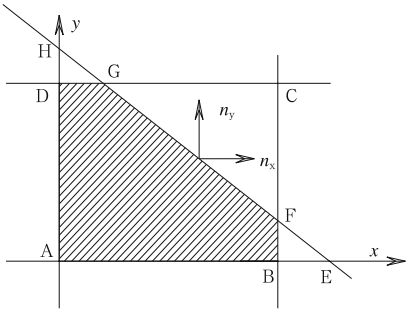

Fig.1. Sketch of free surface reconstruction and flow volume propagation.

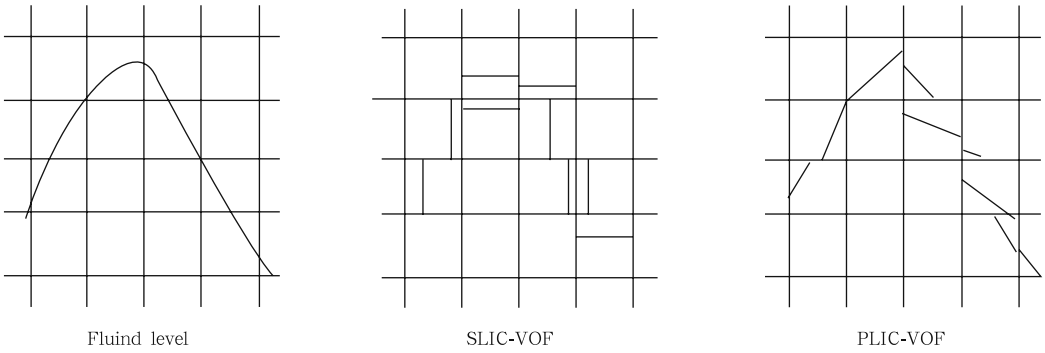

Fig.2. The free surface reconstruction methods of SLIC-VOF and PLIC-VOF.

2.3 *Boundary conditions and computational technique*

The numerical model adopts the *source function wave generating method* (Brorsen et al., 1987). The bottom boundary uses a no-slip boundary condition. The right and left boundary conditions assume as a solid-reflective wall and an absorbing wave-maker boundary condition, respectively. Eqs (2) and (6) are solved by SOR iteration method and corrected with pressure-velocity adjustment techniques.

3 Outline of the experiment

An experiment is conducted to examine the numerical model. Figure 3 is the sketch of the wave flume in the School of Hydraulic Engineering, Changsha University of Science and Technology. The flume is 60.0 m long, 0.5 m wide, and 0.8 m high. It is outfitted with a servo-hydraulically actuated, piston-type wave maker and wave energy absorber (Fig. 3). Wave surface elevation is measured using the capacitance-type wave probes with excellent long-term stability and

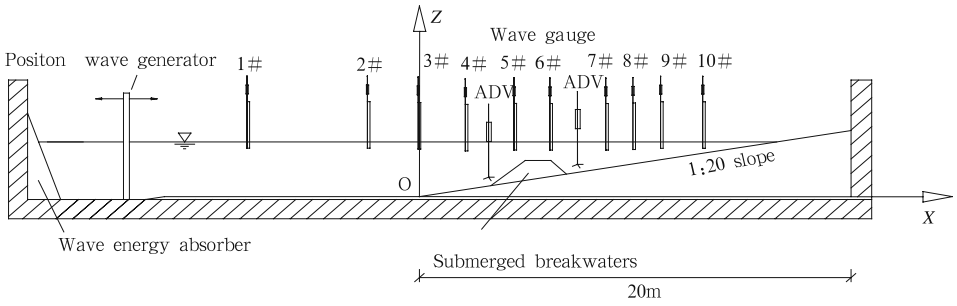

Fig.3. Sketch of the flume.

linear calibration curve. The SonTek 16-MHz MicroADV (Acoustic Doppler Velocimeter) is used to measure the three-dimension (3D) water velocity.

A 1/20 slope is placed at one side of the flume. The reference frame, with which the origin begins at the slope jumping-off point, is established. The vertical direction is defined as z-axis. The x-axis is direction for wave propagation. The trapezoidal-type submerged breakwater is located at X=3.0 m on the sloping bed. The size of submerged breakwater is 10 cm crest wide, 1∶2 gradient of front slope, 1∶1 gradient of back slope, and 8 cm depth of submergence. The location of wave gauges is shown in Table 1 and the location of ADV is shown in Table 2.

The regular wave is used as incident wave in the experiment. The wave periods are from 0.9 to 1.9 sec, wave heights are from 2.2 cm to 8.1 cm, and the water depth is 0.3 m.

Table 1. Location of wave gauges

Wave gauge	1#	2#	3#	4#	5#	6#	7#	8#	9#	10#
x/m	–10.0	–1.5	0.0	1.0	2.0	2.5	3.14	3.5	4.5	5.5

Table 2. Location of ADV

Coordinate	1#	2#	3#	4#	5#	6#	7#	8#
X/m	0.0	1.0	2.0	2.5	2.8	3.0	3.4	4.0

The numerical model uses regular rectangular mesh with 0.005 m of Δy, and 0.01 m of Δx. The total time of numerical simulation is 60 s, and time step used in the model is 0.5 s. Figure 4 demonstrates the numerical and experimental results of the horizontal and vertical velocities at 1.0 cm height above of bed

at the beginning of slope under regular wave (H=8.1 cm and T=1.4 s). Figure 5 shows the numerical and experimental results of wave surface elevation under regular wave (H=8.1 cm and T=1.4 s). It indicates that the calculation capacity to reproduce the experimental results is good and that the numerical model is able to handle the wave-submerged breakwaters interaction problem.

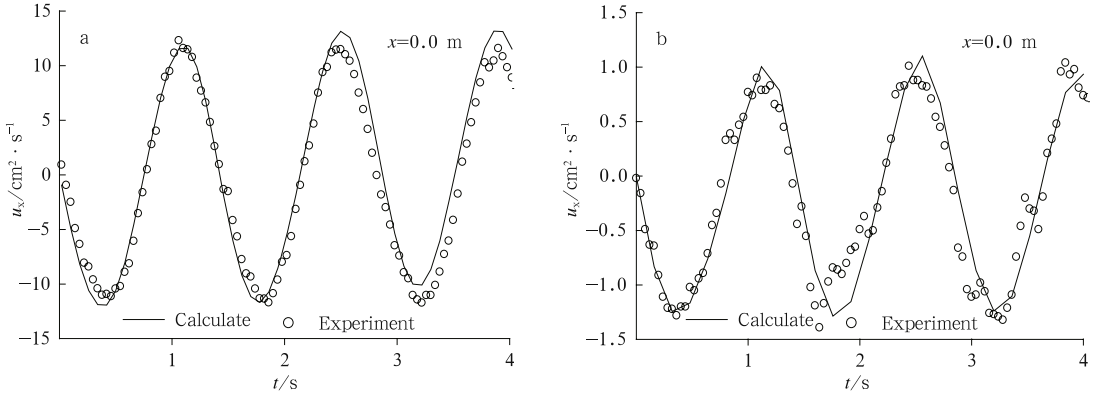

Fig.4. Time series of (a) horizontal and (b) vertical velocities (h=0.30 m; T=1.4 s; H=8.1 cm).

4 Results and discussions

4.1 *Wave profile*

Figure 5 shows the numerical and experimental results of wave surface elevation under regular wave (H=8.1 cm and T=1.4 s). The observations can be described as follows. The symmetrical wave profile at the beginning of the slope shows that the nonlinear effect is weak. When wave propagates on the slope, influenced by shoaling as the depth of water decreases, the wave profile becomes unsymmetrical, the transmitted wave height augments, and the wave crest turns steeper. When wave propagates over the submerged breakwaters, the nonlinear effect noticeably strengthens as the depth of water suddenly decreases. Meanwhile, higher harmonics is generated and the energy in lower harmonics is transferred into higher harmonics. As the relative depth of water increases behind the breakwater, the nonlinear effect becomes weak. The energy in bound harmonics is transferred into free higher harmonics. Free wave satisfies the dispersion relation and travels more slowly than incident wave because of their smaller wave periods, free wave detach themselves from the main wave crest as the wave train propagates. At the same time, the wave profile becomes more unsymmetrical and the wave crest turns steeper. When wave continues passing on the slope, the wave profile becomes much more unsymmetrical, the wave crest turns much steeper. In the crush zone, the wave height decreases when wave is breaking.

In order to characterize the changes of wave profile, three parameters (namely, the value of period of wave forehead crest T' divided by period of wave back crest T'', the value of period of wave crest (T'+T'') divided by period of wave T, the value of wave crest height η_c divided by wave hollow height η_t), have been utilized as shown in Fig.6(a). The values of T'/T'' and $(T'+T'')/T$ are parameters of lengthway asymmetry, and the value of η_c/η_t is the parameter of axial asymmetry. If T'/T''=1.0, $(T'+T'')/T$=0.5, and η_c/η_t=1.0, it means a symmetrical wave profile.

Figures 6b–d shows the changes of parameters of wave profile asymmetry under regular wave on the slope. All three parameters begin to alter at the submerged breakwater, which means that wave profile becomes more asymmetrical.

4.2 *Velocity field*

The vortex is likely to occur or dissipate near the submerged breakwater as boundary layer develops. Figure 5 illustrates the numerical results of velocity field near the submerged breakwater on the slope under regular wave. The observation is given as follows.

When wave crest propagates at front of submerged breakwater (Fig.7a), the anticlockwise vortex generates in the offshore bed on the slope. At the same time, the clockwise vortex also generates in the onshore bed and extends to the offshore corner of the breakwater. When wave crest propagates at the top of breakwater (Fig.7b), the anticlockwise vortex extends to the breakwater crest and dissipates in the offshore bed on the slope. When wave crest propagates at the

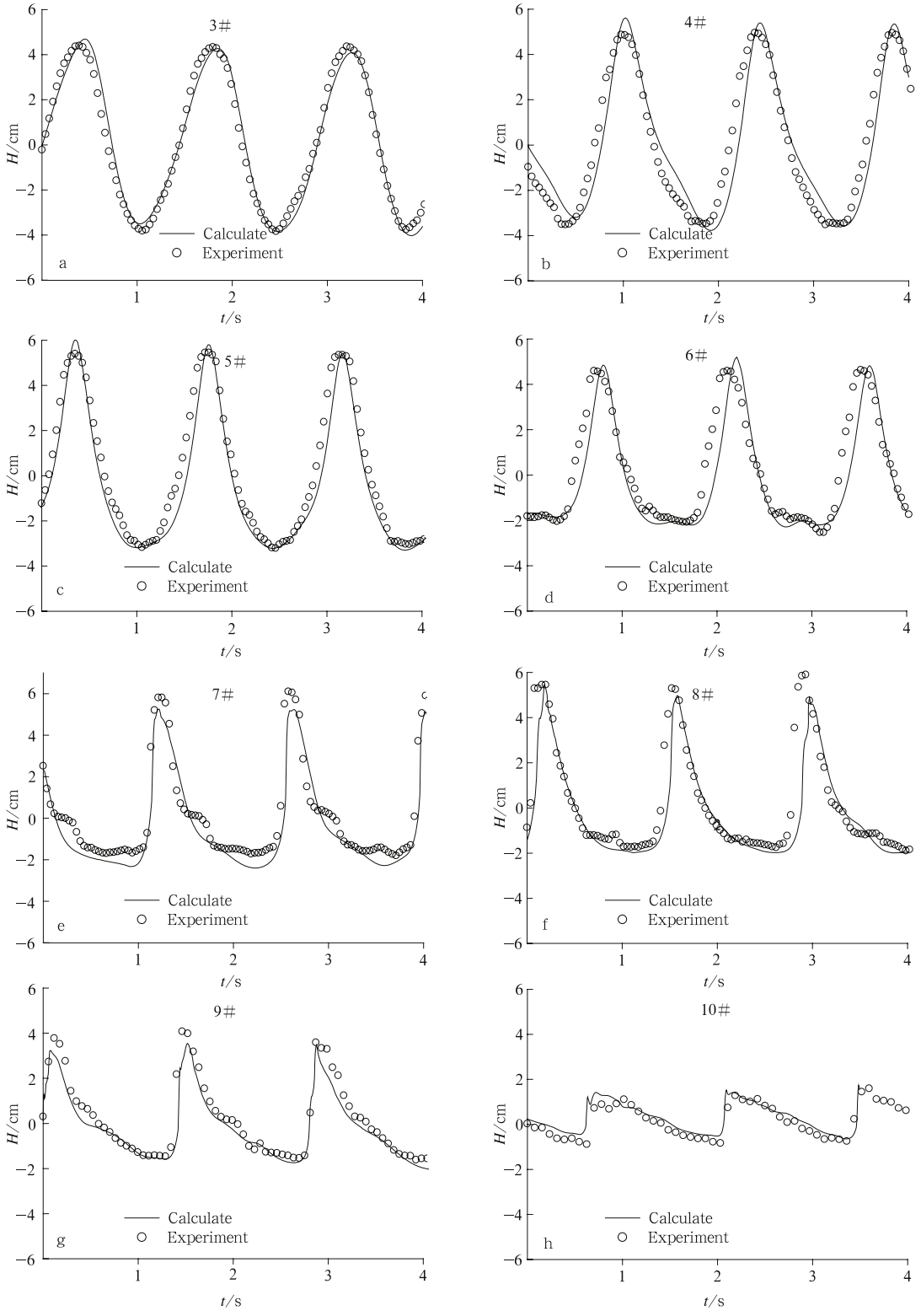

Fig.5. Time series of water surface displacement under regular wave (h=0.30 m; T=1.4 s; H=8.1 cm).

back of breakwater (Fig.7c), the anticlockwise vortex extends to the onshore bed. Meanwhile, the clockwise vortex begins to generate in the offshore bed. When wave hollow propagates at the top of breakwater (Fig.7d), the clockwise vortex begins to dissipate in the offshore bed and generates in the onshore bed

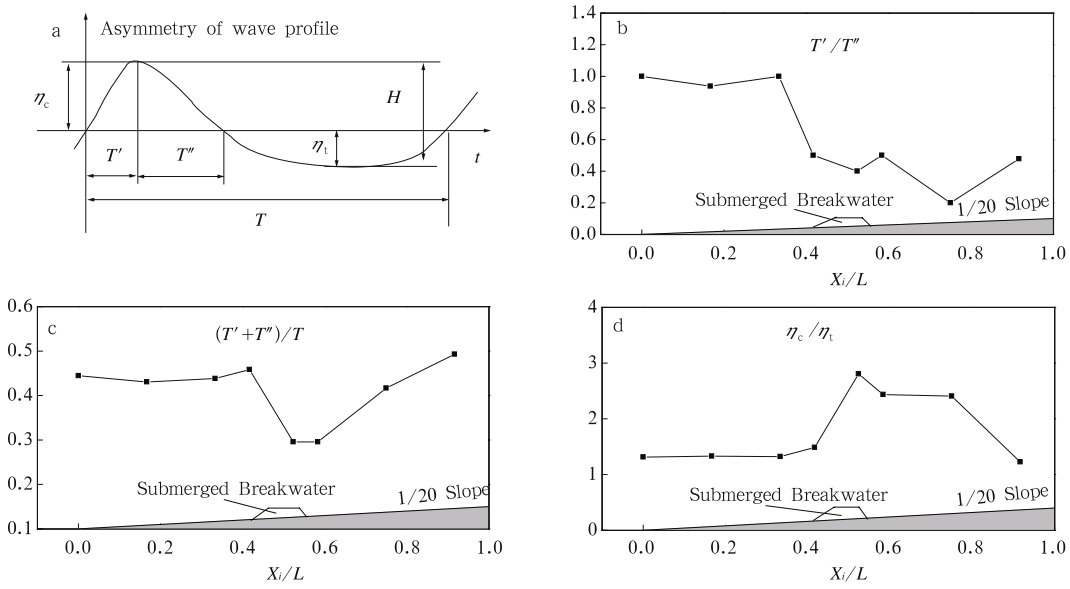

Fig.6. Parameters of asymmetry of wave profile under regular wave (h=0.30 m; T=1.4 s; H=8.1 cm).

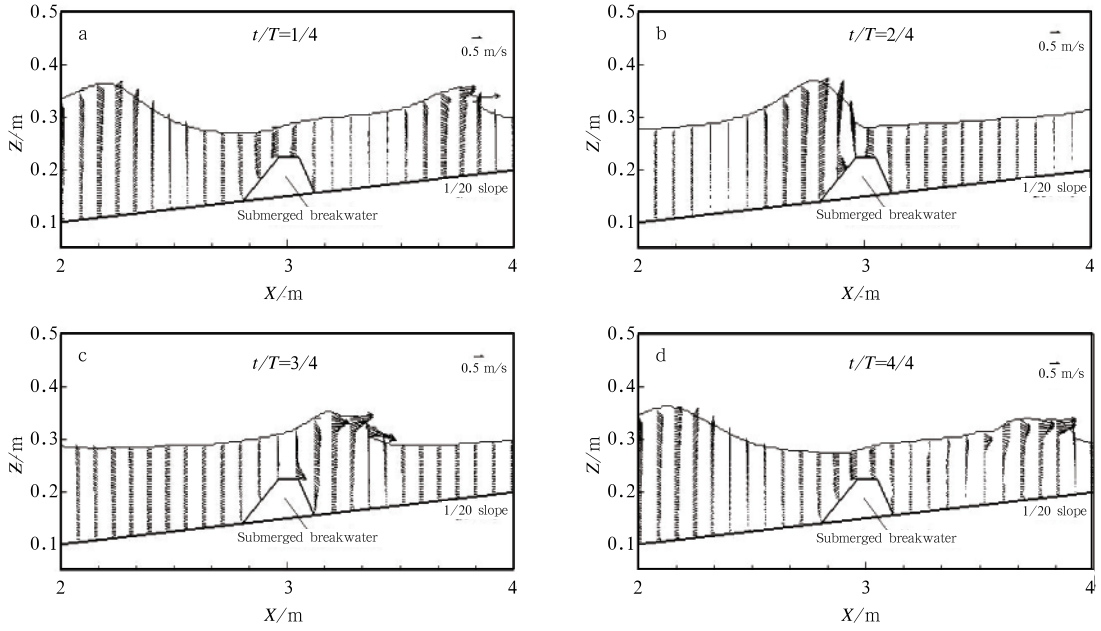

Fig.7. Velocity field near the submerged breakwater on the slope under regular wave. (h=0.30 m; T=1.3 s; H=7.1 cm).

on the slope.

As can be seen, some energy is transferred into the anticlockwise vortex when wave crest propagates over breakwater. Therefore, the anticlockwise vortex generates and the clockwise vortex dissipates. In another case, some energy is transferred into the clockwise vortex when wave hollow propagates over breakwater. Thereby, the clockwise vortex generates and the anticlockwise vortex dissipates.

4.3 *Turbulent kinetic energy*

When fluid propagates breakwater, the velocity of flow increases and turbulence occurs because of the influence of viscidity and nonlinear effect. The numerical model including nonlinear $k-\varepsilon$ model focuses the characteristics of flow field. The result shows the changes of turbulent kinetic energy near the breakwater on the slope.

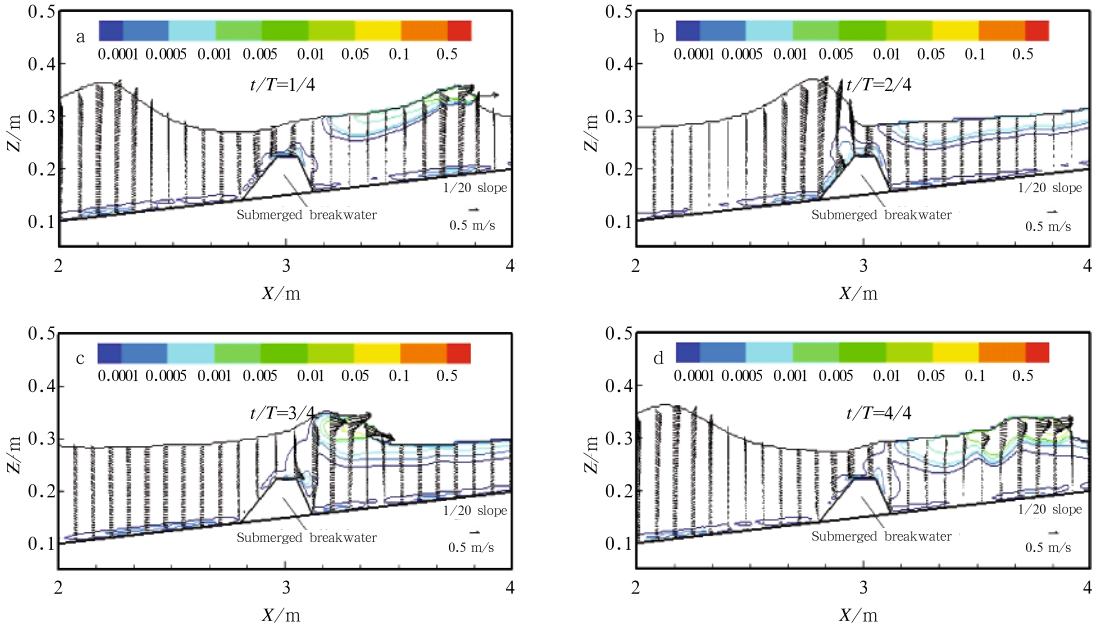

Fig.8. Turbulent kinetic energy near the submerged breakwater on the slope under regular wave. (h=0.30 m; T=1.3 s; H=7.1 cm; Unit: m^2/s^2)

The turbulent kinetic energy near the submerged breakwater is illustrated by Fig.8. The observations are described as follows. When wave crest propagates at front of submerged breakwater (Fig.8a), a remarkable change in velocity makes the turbulent kinetic energy increase on the top of breakwater as the clockwise vortex generates. When wave crest propagates at the top of breakwater (Figs 8b and c), the most turbulent kinetic energy occurs at the wave crest. Because the anticlockwise vortex generates and extends to breakwater crest, the turbulent kinetic energy increases on the top of breakwater. As wave crest propagates at the back of breakwater, the most turbulent kinetic energy shifts from offshore breakwater bed to onshore breakwater bed. When wave hollow propagates on the top of breakwater (Fig.8d), the turbulent kinetic energy begins to increase as the clockwise vortex increases.

The results of observation suggest that the most turbulent kinetic energy always occurs on the top of breakwater. The turbulent kinetic energy increases as the vortex increases. Meanwhile, the turbulent kinetic energy decreases because the vortex is restricted.

4.4 *Turbulent dissipation*

Figure 9 shows the calculated result of turbulent dissipation near the submerged breakwater on the slope under regular wave. The tendency of turbulent dissipation varies similarly to that of turbulent kinetic energy. Due to the intense turbulent kinetic energy on the top of breakwater, wave energy dissipation makes the turbulent dissipation increase.

4.5 *Eddy viscosity*

It is anticlockwise when eddy viscosity is a positive value, while it is clockwise when eddy viscosity is a negative value. Eddy viscosity defines:

$$\omega = \frac{\partial v}{\partial x} - \frac{\partial u}{\partial y}. \tag{7}$$

As indicated in Fig.10, eddy viscosity near the submerged breakwater on the slope under regular wave is given. When wave crest propagates at front of submerged breakwater (Fig.10a), the anticlockwise eddy viscosity generates in the offshore bed on the breakwater. Meanwhile the clockwise eddy viscosity begins to diminish and vanish finally. When wave crest propagates on the top of breakwater (Fig.10b), the anticlockwise eddy viscosity increases and extends. As wave crest propagates at the back of breakwater (Fig.10c), the anticlockwise eddy viscosity shifts from offshore breakwater bed to onshore breakwater bed. When wave hollow propagates on the top of breakwater (Fig.10d), the clockwise eddy viscosity begins to increase and extend in the onshore breakwater bed. The tendency of turbulent kinetic energy, turbulent dissipation and eddy viscosity changes in a same way.

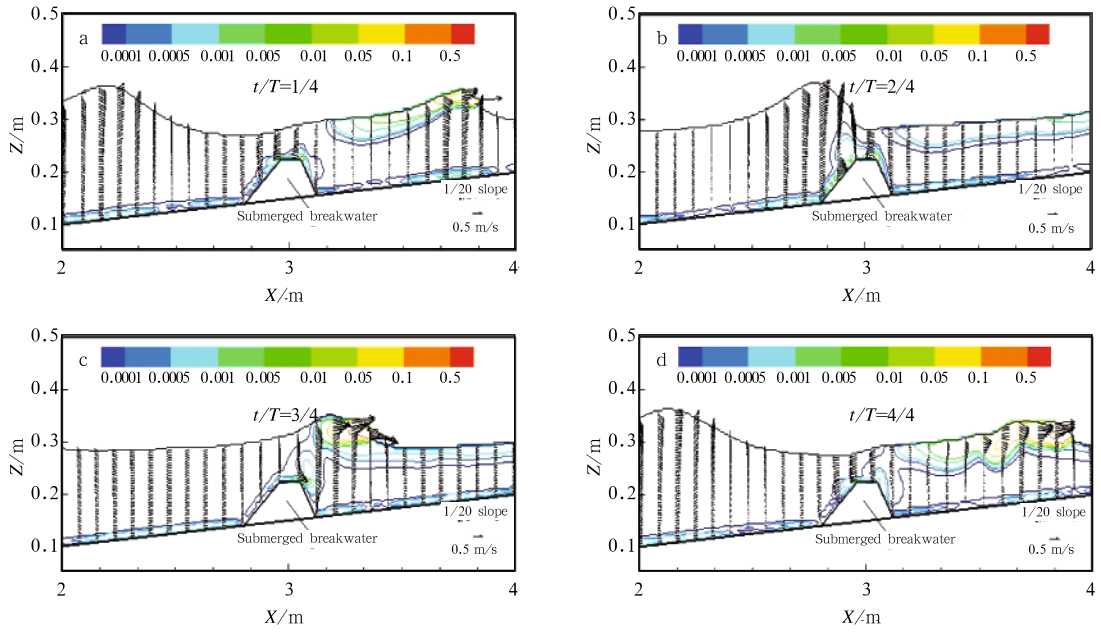

Fig.9. Turbulent dissipation near the submerged breakwater on the slope under regular wave. (h=0.30 m; T=1.3 s; H=7.1 cm; Unit: $m^3 \cdot s^{-3}$).

The numerical result shows that PLIC-VOF model used in this study is effective and can compute the wave and flow field precisely. However, numerical model does not precisely simulate velocity distribution in wave boundary layer due to the influence of structured grid. The velocity distribution in wave boundary layer is very vital to the theoretical research and practice. One method to solve this problem is to transform structured grid into unstructured grid. The unstructured grid is very suitable to handle problems with complex geometries. The future development of the numerical model need to deal with this issue.

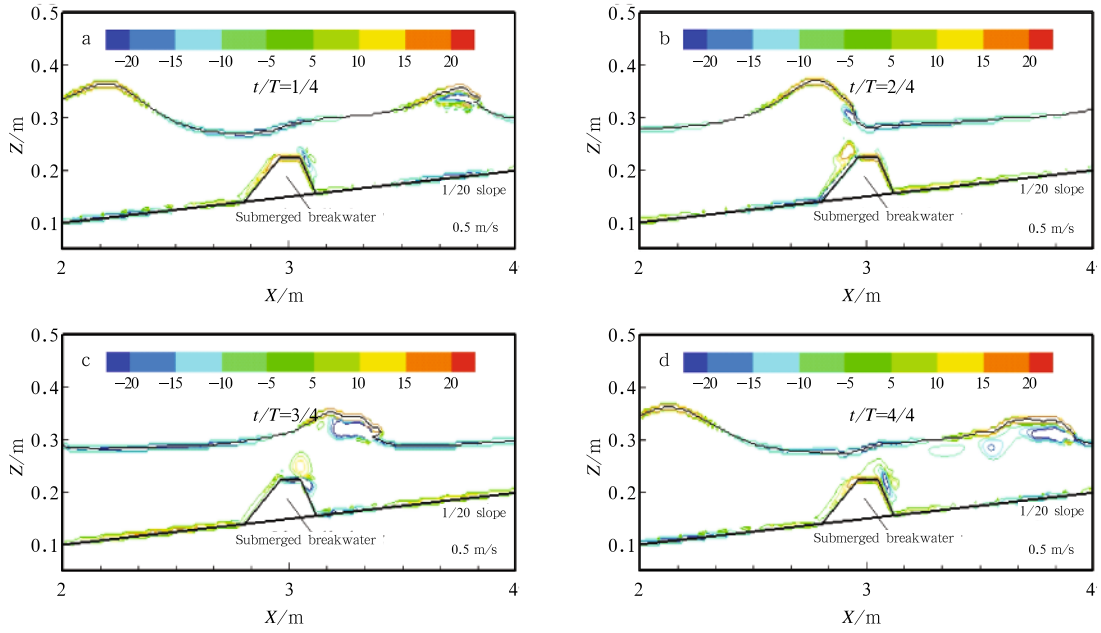

Fig.10. Eddy viscosity near the submerged breakwater on the slope under regular wave. (h=0.30 m; T=1.3 s; H=7.1 cm; Unit: s^{-1}).

4.6 *Wave energy*

The wave energy spectrum at front, back toe and back of submerged breakwater under regular wave are presented in Fig.11. Wave energy spectrum is calculated by Fast Fourier Transform method. Fig.12 also shows the changes of wave energy on the slope under regular wave. The little second harmonic energy at the beginning of the slope indicates that the nonlinear effect is weak. Influenced by shoaling as the depth of water decreases when wave propagates on the slope, the fundamental energy significantly decreases and second harmonic energy increases at the front of slope. When wave propagates at the submerged breakwater, the nonlinear effect visibly strengthens as the depth of water suddenly decreases. Meanwhile, higher harmonics are generated and the energy in lower harmonics is transferred into higher harmonics. The fundamental energy rapidly decreases. At the back of breakwater, as the relative depth of water increases behind the breakwater, the nonlinear effect becomes weak. The energy in harmonics decreases. In the crush zone, all the fundamental and higher harmonic energy increase because of intense turbulence and eddy included frictional loss.

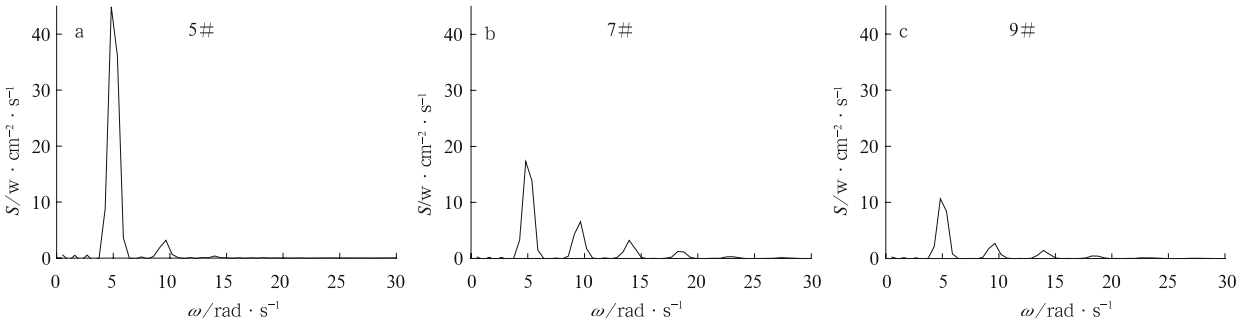

Fig.11. Wave energy spectrum at (a) front, (b) back toe, (c) back of submerged breakwater under regular wave (h=0.30 m; T=1.4 s; H=8.1 cm)

The analysis indicates that the function of the submerged breakwater absorbing wave partly is that energy in lower harmonics is transferred into higher harmonics because of shoaling on the top of submerged breakwater, and partly is that the development of boundary layer makes turbulent kinetic energy, turbulent dissipation and eddy viscosity near breakwater increase to dissipate wave energy (Fig. 12). There has a process that all higher harmonics increases nearby the submerged breakwater, and so do the turbulent kinetic energy, turbulent dissipation and eddy viscosity.

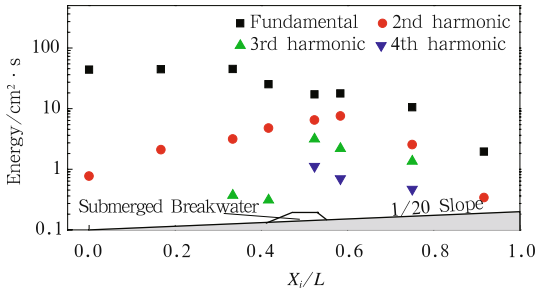

Fig.12. Changes of wave energy on the slope under regular wave (h=0.30 m; T=1.4 s; H=8.1 cm)

5 Conclusions

The characteristics of flow field and wave propagation over submerged breakwater on a sloping bed are investigated by numerical model in this study. The governing equations of the vertical two-dimensional model are the Reynolds Averaged Navier Stokes equations. The Reynolds stress terms are closed by a nonlinear $\kappa-\varepsilon$ turbulence transportation model. The free surface is traced through the PILC-VOF method. The proposed numerical model is examined by comparison with the experimental results. By the analyses of its applicability the proposed numerical model is proved to be effective in predicting characteristics of flow field and wave propagation near submerged breakwater on a sloping bed.

Analyses of the changes of wave surface elevation and three parameters of wave profile asymmetry shows that wave profile may become more asymmetrical when wave propagates over breakwater. When wave crest propagates over breakwater, the anticlockwise vortex may generate. Contrarily, when wave hollow propagates over breakwater, the clockwise vortex may generate. If the anticlockwise vortex generates,

the clockwise vortex could dissipate. Meanwhile, the influenced zone of vortex, created by wave crest, is larger than that created by wave hollow.

All the maximum values of turbulent kinetic energy, turbulent dissipation and eddy viscosity may occur on the top of breakwater. The turbulent dissipation and eddy viscosity increase as the turbulent kinetic energy increases. The turbulent kinetic energy decreases because the vortex is restricted under current experimental condition.

All of the higher harmonics may increase at the front of breakwater and rapidly decrease at back of breakwater. Wave energy may rapidly decrease at the breakwater because the turbulent dissipation increases and energy in lower harmonics is transferred into higher harmonics.

Acknowledgements

Thank assistant professor Hu Shixiong (Department of Geography, East Stroudsburg University of Pennsylvania) for his help.

References

Brorsen Mlehael, Larsen Jesper. 1987. Source generation of nonlinear gravity waves with the boundary integral equation merhod. Coastal Engineering, 11: 93–213

Chen Jie, Jiang Changbo, Cao Yonggang, et al. 2008. Experimental study of transmission coefficient of waves over submerged breakwater on a sloping bed. Sciencepaper Online, 7: 516–523

Chen K H, Chen J T. 2006. Adaptive dual boundary element method for solving oblique incident wave passing a submerged breakwater. Computer Methods in Applied Mechanics Engineering, 196: 551–565

Chen Kue-Hong, Chen Jeng-Tzong, Lin Sheng-Yih, et al. 2004. Dual Boundary Element Analysis of Normal Incident Wave Passing a Thin Submerged Breakwater with Rigid, Absorbing, and Permeable Boundaries. Journal of Waterway, Port, Coastal, and Ocean Engineering, 179–190

Chiranjeevi Rambabu A, Mani J S. 2005. Numerical prediction of performance of submerged breakwaters. Ocean Engineering, 32: 1235–1246

Cho Yong-Sik, Lee Jong-In, Kim Young-Taek: 2004. Experimental study of strong reflection of regular water wave over submerged breakwaters in tandem. Ocean Engineering, 31: 1325–1335

Dimitrios G Stamos, Muhammad R Hajj, Demetri P Telionis: 2003. Performance of hemi-cylindrical and rectangular submerged breakwaters. Ocean Engineering, 30: 813–828

Dimitrios G Stamos, Muhammad R Hajj. 2001. Reflection and transmission of wave over submerged breakwaters. Journal of Engineering Mechanics, 3: 99–105

Jiang Changbo, Chen Jie, Xiao Zheng, et al. 2008. Wave propagation over submerged breakwater on a sloping bed. Journal of Changsha University of Science & Technology, 3: 47–51

Jeng D S, Schacht C, Lemckert C. 2005. Experimental study on ocean wave propagating over a submerged breakwater in front of a vertical seawall. Ocean Engineering, 32: 2231–2240

Hur Dong-Soo. 2004. Deformation of multi-directional random wave passing over an impermeable submerged breakwater installed on a sloping bed. Ocean Engineering, 31: 1295–1311

Hur Dong-Soo, Kawashima N, Iwata K. 2003. Experimental study of the breaking limit of multi- directional random wave passing over an impermeable submerged breakwater. Ocean Engineering, 30: 1923–1940

Hakeem K Johnson, Theophanis V Karambas, Ioannis Avgeris, et al., 2005. Modeling of wave and currents around submerged breakwaters. Coastal Engineering, 52: 949–969

Hakeem K, Johnson. 2006. Wave modeling in the vicinity of submerged breakwaters. Coastal Engineering, 53: 39–48

Inigo J Losada, Javier L Lara, Nicolas Garcia. 2003. 2-D Experimental and numerical analysis of wave interaction with low-crested breakwaters including breaking and flow recirculation. Coastal Structures, 863–875

Losada I J, Silva R, Imada M A. 1996. 3-D non-breaking regular wave interaction with submerged breakwaters. Coastal Engineering, 28: 229–248

Losada I J, Silva R, Imada M A. 1996. Interaction of non-breaking directional random wave with submerged breakwaters. Coastal Engineering, 28: 249–266

Liu Cheng, Liu Xiaoping, Jiang Changbo. 2005. Numerical simulation of wave field near Submerged Bars by PLIC-VOF Model. China Ocean Engineering, 19(3): 509–518

Muni Reddy M G, Sannasiraj S A, Natarajan R. 2007. Numerical investigation on the dynamics of a vertical wall defenced by an offshore breakwater. Ocean Engineering, 34: 790–798

Nobuhisa Kobayashi, Leslie E Meigs, Takao Ota, et al. 2007. Irregular breaking wave transmission over submerged porous breakwater. Journal of Waterway, Port, Coastal, and Ocean Engineering, 133: 104–116

Norimi Mizutani, Ayman M Mostafa, Koichiro Iwata. 1998. Nonlinear regular wave, submerged breakwater and seabed dynamic interaction. Coastal Engineering, 33: 177–202

Ronald J Cox, Mojtab a Tajziehchi. 2005. 2D Experimental modeling of hydrodynamic effects of submerged breakwaters. Coastal Dynamics, 1–12

Stephan T Grilli, Miguel A Losada, Francisco Martin. 1994. Characteristics of solitary wave breaking induced by breakwaters. Journal of Waterway, Port, Coastal, and Ocean Engineering, 120(1): 74–92

Wang Y X. 1995. Numerical wave channel with absorbing wave-maker. China Ocean Engineering, 9(2): 149–160

Wang Y X, Zang J, Qiu D H. 1999. Numerical Model of Cnoidal Wave Flume. China Ocean Engineering, 13(4): 391–398

Zhou Yuanheng, Chen Zhijie, Lu Haibin, et al. 2005. Numerical simulation of nonlinear wave interaction with submerged porous breakwater. Port & Waterway Engineering, 3: 8–12